SUPPLEMENTAL MATERIAL

Progenitor cells

Blood collection and isolation of cells. Mononuclear cells were obtained from peripheral blood (100 mL), as described previously[1-5]. Late EPC were obtained from cells collected 3 weeks after the baseline procedure (induction of RAS), and subsequently cultured for 3 weeks, while early EPC were obtained from cells collected and cultured 7 days before the in vivo CT studies. To obtain the cells, animals were sedated with IM telazol (5 mg/kg) and xylazine (2 mg/kg), blood drawn from the femoral vein (100 ml) under sterile conditions, and then divided in heparinized Falcon tubes placed on ice. Mononuclear cells were isolated from the blood by the density gradient method[3, 6] using Histopaque 1077 (Sigma, St. Louis) at 1600 rpm for 25 min, washed with PBS, treated with ammonium chloride (Stem Cell Technologies, Vancouver, BC) to eliminate red blood cells. Cells were re-suspended in EGM-2 plus EGM-2 Singlequot medium (Cambrex, Walkersville, MD). This medium contains multiple growth factors including human VEGF A, fibroblast growth factor-2, endothelial growth factor, insulin-like growth factor-1, and ascorbic acid, as well as gentamycin and amphotericin B. Cells were plated on 6-well plates (Corning Incorporated, Corning, NY) coated with fibronectin (1μg/cm^2, Sigma, St. Louis, MO), with initial seeding density standardized at 4x10^6 cells per well. After 2 days of culture, non-adherent cells were removed and the media changed daily for 1 week, and every other day for the remaining time. The attached cell population at days 4-10 is usually mixed with both round and spindle cells that exhibit many characteristics of EPC, but little proliferative capacity. Late EPC colonies typically sprout around days 11-18, and are comprised of larger cells with mature endothelial cell culture characteristics (cobblestone monolayer, contact inhibition, and rapid proliferation)[4]. Cultures were examined by light microscopy and samples assayed for number,

function, and phenotyped before delivery.

Colony forming unit counting. Colonies consisting of multiple thin, flat cells emanating from a central cluster of rounded (and some spindle-shaped) cells were counted after 7 days of culture in 10 field under (x20) microscope, and expressed as colonies per cm^2 [7, 8] **(Figure 1s-top right)**.

Characterization of EPC marker expression. Immuno-fluorescence and Western blotting (see below) were used to determine cellular phenotype [6]. For immuno-fluorescence, cells were incubated with primary antibodies (all 1:50) against CD34 (R&D Systems, MN, Cat# AF3890, NS0-derived rpCD34), CD14 (Serotec, Oxford, UK Cat#MCA1218, Clone: MIL-2), CD133 (GeneTex, TX, Cat# GTX16518, Clone: RB1784), KDR (Santa Cruz, CA, Cat# sc-504, Clone: C-1158), and Oct-4 (1:50, Lifespan Biosciences, Seattle, WA, Cat# LS-B85, Clone: Octamer-binding Transcription Factor 3A (POU5F1)) for 1h at room temperature. FITC-goat anti-mouse or anti-rabbit IgG (or Texas red conjugated) secondary antibodies (ZYMED Laboratories, South San Francisco, CA) were incubated for 30 min at room temperature. To enable visualization of nuclei, DAPI mount media (Santa Cruz, CA) was used. Isotype identical IgG antibodies served as negative controls. Slides were examined under fluorescence microscopy **(Figure 1s-left)**.

EPC function were tested using several accepted tests [9].

Acetylated LDL uptake: Cells were incubated with DiI-labeled ac-LDL (Molecular Probes, Eugene, Ore), samples examined with an inverted fluorescence microscope (Nikon), and fluorescent cells identified as EPC **(Figure 2s-top)**.

EPC migratory function: VEGF-induced cell migration was examined using a modified Boyden chamber[8]. A 24-well Transwell apparatus (Coster, Corning Inc., Corning, NY) was used, with each well containing a 6.5-mm polycarbonate membrane with 8-µm pores. Cells ($4x10^4$) were placed on the membrane, and the chamber immersed in a plate filled with growth factor-free

EBM-2 culture media, with addition of 2000 pg/ml human VEGF165 (R&D System, Minneapolis, MN). After incubation for 24-h, the membrane was washed briefly with PBS, and its upper side wiped gently with a cotton ball. The membrane was then removed and mounted with DAPI fluorescence medium (Santa Cruz, CA). EPC migration was evaluated by counting the migrated cells in 4 random high-power (x40) fluorescence microscope fields **(Figure 2s-bottom-left)**.

Proliferation Assay: Late EPC were seeded at 3×10^3/well in 96-well flat-bottomed plates in EGM-2 medium containing 2% FCS and allowed to adhere for 2 h. After 24h culture with or without concurrent exposure to different concentration of vitamins, the proliferative activity was determined by MTS assay (CellTiter 96 Non-Radioactive Cell Proliferation Assay; Promega, Madison, WI**, Figure 2s bottom-right**), which monitors the number of viable cells, according to vendor instructions. Briefly, MTS solution was added at 20 µl/well and, after 4 h culture, the conversion of MTS to formazan was measured in a plate reader at 490 nm.

Matrigel Tube Formation Assay: assessed the ability of EPC to incorporate into endothelial cells and form vascular structures [8]. Matrigel (BD Biosciences, Bedford, MA) was spread onto 24-well plates (Coster, Corning Inc., Corning, NY)) and allowed to polymerize for 15 min at 37°C. For the assay, early and late EPC were marked with DiI (Molecular Probes) and mixed with human umbilical endothelial cells (HUVEC, PromoCell, Heidelberg, Germany. DiI-labeled EPC ($1x10^4$) and HUVEC ($4x10^4$) were plated together and incubated at 37°C for 24h with EGM-2 culture medium. Tube length, and number, as well as the cells incorporated into HUVEC tubes [8], were counted in 4 random (x20) fields per subject and measured using MetaMorph® image analysis software (Meta Imaging Series 6.3.2, Allentown, PA). Experiments were done in triplicate and observers blinded to cell type and group **(Figure 3s)**.

Growth factor and cytokine measurement[2]

To determine the ability of EPC generating and secreting growth factor and cytokine, at day 20, growth factor free media was used and cultured for 24h. Media was collected for measurement of VEGF level by ELISA kit (**Figure 4s-left**, R & D System, MN). Cells were then homogenized, and expression of VEGF and eNOS were evaluated by Western Blotting, as previously published (**Figure 4s-right**).

Preparation of cells for delivery [10]. Cells were labeled with both a fluorescent membrane dye (CM-DiI) as well as fluorescent beads. CM-DiI (5µl/ml) was added to the culture medium and incubated for 30 min at 37°C. Fluoresbrite plain 2 µm YG (yellow-green) polymeric beads (Polysciences, Warrington, PA) were added at a 1:25 cell-to-microspheres ratio, and incubated 75 min at 37 °C. These beads exhibit exceptionally high brightness combined with photostability and high signal to noise ratio, thereby allowing prolonged detection. Cells were detached by incubation with 0.25% trypsin/1 mmol/L EDTA, followed by forceful pipetting and washing with PBS x3, and were kept in 10 ml PBS on ice until delivery (10^6 cells /ml).

EPC delivery. A mixture of early and late EPC were prepared and infused distal to the stenosis after 6 weeks of RAS, based on previous reports demonstrating a synergistic effect in promoting neovascularization when both cell types are administered[1]. Briefly, under anesthesia, sterile conditions, and fluoroscopic guidance, a 6 mm PTCA balloon catheter was advanced into the renal artery over a 0.014" guide wire, and engaged proximal to the stenosis. The balloon was inflated and expanded to full diameter, and 10 mL labeled cells (10^6 cells/mL) suspended in saline manually injected slowly through the baloon [4, 5]. After injection, the catheter was immediately flushed with 10 mL of saline, the baloon kept inflated for another 5-10 min to prevent cell washout, and then removed. RAS remained unchanged.

EPC localization and retention was estimated from the engrafted cells observed in the kidney section[11]. Labeled cells were manually counted under fluorescence microscopy in 20 frozen 5μm renal cross-sections counterstained with hematoxylin (**Figure 5s**). The total area of each cross-section was obtained using an image-analysis program (MetaMorph, Meta Imaging Series 6.3.2, Allentown, PA), and the number of cells per mm^2 averaged and multiplied by the section thickness. This (average number of cells/mm^3) was in turn multiplied by MDCT-derived renal volume (mm^3) to obtain the total number of EPC in the kidney, and divided by the number of injected cells (i.e., retention rate).

EPC engraftment: Double fluorescence of CM-DiI (labeled EPC before delivery) and immunofluorescences of CD31, cytokeratin, or Oct-4 were determined to investigate the engraftment of EPC into endothelial or tubular structures, their phenotype changes, and their relationship with endogenous stem cells. For this purpose, frozen slices (5 μm) from the stenotic kidney were incubated with CD31 (AbD Serotec, Cat#MCA1747, Clone: LC1-9), cytokeratin (AbD Serotec, Cat# MCA1907, Clone: AE1/AE3), or Oct-4 (1:50, Lifespan Biosciences, Seattle, WA) antibodies for 1h at room temperature. FITC-goat anti-mouse or rabbit IgG secondary antibodies (Zymed Laboratories, South San Francisco, CA) were incubated for 30 min at room temperature. To enable visualization of nuclei, DAPI mount media (Santa Cruz, CA) was used. Isotype identical IgG antibodies served as negative controls. Slides were examined under fluorescence microscopy. Peritubular capillary density was also evaluated using CD31 stained slides.

Micro-CT: A saline-filled cannula was ligated in a segmental artery perfusing the intact end of the stenotic kidney, and infusion of 0.9% saline (containing 10 units/ml heparin) was perfused under physiological perfusion pressure (Syringe Infusion Pump 22, Harvard Apparatus,

Holliston, MA). After 10-15 minutes the saline infusion was replaced with infusion (0.8 ml/min) of an intravascular contrast agent, which was a freshly mixed radio-opaque silicone polymer, containing lead chromate (Microfil MV122, Flow Tech, Inc., Carver, MA) until the polymer drained freely from the segmental vein. Then, a lobe of the polymer-filled tissue was trimmed from the kidney, placed in 10% buffered formalin, glycerinated, and encased in paraffin. The kidney samples were scanned at 0.5˚ increments using a micro-CT scanner, as previously described[12-15] and the 3D volume images were reconstructed. The images consisted of cubic voxels of 20 μm on a side, and were displayed at 20 μm cubic voxels for subsequent analysis.

Renal protein expression and Western Blotting

Immunohistochemistry: staining was performed in 5 μm frozen or unstained mid-hilar renal cross-sections to assess the expression of integrin β_3 (Chemicon International, CA, 1:80, Clone BV4), and α-Smooth muscle actin (α-SMA, Dako, CA,1:50, cat#M0851, clone 1A4). The secondary antibody, IgG Envision Plus (Dako), was followed by staining with the Vector NovaRED substrate kit (Vector Laboratories, Burlingame, CA), following vendor's instructions. In addition, Oct-4 (1:50, Lifespan Biosciences, Seattle, WA, Clone: POU5F1) staining was performed in paraffin fixed slides incubated with primary antibody overnight at 4°C, washed by PBS, incubated with the secondary antibody, VECTASTAIN® Elite ABC kit (Vector Laboratories, Burlingame, CA), and followed by staining with the Vector DAB substrate kit (Vector Laboratories, Burlingame, CA). Nuclear counter staining was achieved using nuclear fast red (Vector Laboratories, Burlingame, CA).

TUNEL: Renal sections were stained using the DeadEnd Fluorometric TUNEL System (Promega, Madison, WI), following manufacturer's instructions. To quantify the frequencies of apoptotic cells, twenty random glomeruli or tubular fields were captured from the kidneys using

a confocal microscope (Zeiss LSM 510, Germany), and apoptotic index defined as the number of positive cells divided by the total number of cells in each field.

Western blotting: standard blotting protocols were followed, as previously described[16], using specific polyclonal antibodies against p-Akt (Clone: Ser 473), p-eNOS, VEGF (Clone 147), HIF-1α (Clone H-206), TGF-β (Clone V), MMP-2 (Clone H-76), TIMP-1 (Clone H-150) (Santa Cruz, CA, 1:200 for all), angiopoietin-1 (Novus Biologicals, CO, 1:500), MMP-9 (Millipore, MA, 1:2,000), and Oct-4 (1:500, Lifespan Biosciences, Seattle, WA Clone: POU5F1). β-actins (Sigma, Saint Louis, MO, 1:500) or GAD(P)H (1:5000, Covance, Emeryville, CA) were used as loading controls. Protein expression was determined in each kidney, and the intensities of the protein bands (one per animal) were quantified using densitometry and averaged in each group.

Data analysis

MDCT analysis: Manually-traced regions of interest were selected in MDCT images in the aorta, renal cortex, medulla, and papilla, and their densities sampled. Time-density curves were generated and fitted with extended gamma-variate curve-fits, and the area enclosed under each segment of the curve and its first moment calculated using the curve-fitting parameters[17]. These were used to calculate renal regional perfusion (ml/minute/g tissue), single-kidney GFR, and RBF, using previously-validated methods[16-21].

Micro-CT analysis: Images were digitized for reconstruction of 3-D volume images, and analyzed with the Analyze® software package (Biomedical Imaging Resource, Mayo Clinic, Rochester, MN). For analysis of the cortex, the three-dimensional tomographic images were oriented so that the z-axis was parallel to the radial vessels. Based on the number of cortical sections, the cortex was tomographically divided into 10 levels obtained at equal intervals, starting at the juxtamedullary cortex. For analysis, levels 1-3 were considered as inner third,

levels 4-7 as middle third, and levels 8-10 as the outer third of the cortex[14]. The spatial density, average diameter, and vascular volume fraction (sum of cross-sectional areas of all vessel /area of the region of interest) of cortical microvessels (diameters <500μm) were calculated in each level. Tortuousity index factor was calculated as we have recently described[12, 13]. Briefly, 1-3 intra-cortical arterioles and their branches were tomographically "dissected" in each pig, the 3D path distance (total length) and linear distance (shortest distance between endpoints) of the main branches were calculated, and the tortuousity index calculated by dividing path distance by linear distance[13].

Histology: Mid-hilar 5 μm cross sections of each kidney (1 per animal) were examined using a computer-aided image-analysis program (MetaMorph®, Meta Imaging Series 6.3.2). In each representative slide, trichrome staining was semi-automatically quantified in 15-20 fields by the computer program, expressed as percentage of staining of total surface area, and the results from all fields averaged[15, 19-22]. Glomerular score (percentage of sclerotic glomeruli) was assessed by recording the number of sclerotic glomeruli out of 100 counted glomeruli[16, 19-21].

References

1. Yoon CH, Hur J, Park KW, Kim JH, Lee CS, Oh IY, Kim TY, Cho HJ, Kang HJ, Chae IH, Yang HK, Oh BH, Park YB, Kim HS. Synergistic neovascularization by mixed transplantation of early endothelial progenitor cells and late outgrowth endothelial cells: the role of angiogenic cytokines and matrix metalloproteinases. *Circulation.* 2005;112:1618-1627.

2. Hur J, Yoon CH, Kim HS, Choi JH, Kang HJ, Hwang KK, Oh BH, Lee MM, Park YB. Characterization of two types of endothelial progenitor cells and their different contributions to neovasculogenesis. *Arterioscler Thromb Vasc Biol.* 2004;24:288-293.

3. Gulati R, Jevremovic D, Peterson TE, Chatterjee S, Shah V, Vile RG, Simari RD. Diverse origin and function of cells with endothelial phenotype obtained from adult human blood. *Circ Res.* 2003;93:1023-1025.

4. Gulati R, Jevremovic D, Peterson TE, Witt TA, Kleppe LS, Mueske CS, Lerman A, Vile RG, Simari RD. Autologous culture-modified mononuclear cells confer vascular protection after arterial injury. *Circulation.* 2003;108:1520-1526.

5. Gulati R, Jevremovic D, Witt TA, Kleppe LS, Vile RG, Lerman A, Simari RD. Modulation of the vascular response to injury by autologous blood-derived outgrowth endothelial cells. *Am J Physiol Heart Circ Physiol.* 2004;287:H512-517.

6. Lin Y, Weisdorf DJ, Solovey A, Hebbel RP. Origins of circulating endothelial cells and endothelial outgrowth from blood. *J Clin Invest.* 2000;105:71-77.

7. Hill JM, Zalos G, Halcox JP, Schenke WH, Waclawiw MA, Quyyumi AA, Finkel T. Circulating endothelial progenitor cells, vascular function, and cardiovascular risk. *N Engl J Med.* 2003;348:593-600.

8. Choi JH, Kim KL, Huh W, Kim B, Byun J, Suh W, Sung J, Jeon ES, Oh HY, Kim DK. Decreased number and impaired angiogenic function of endothelial progenitor cells in patients with chronic renal failure. *Arterioscler Thromb Vasc Biol.* 2004;24:1246-1252.

9. Dzau VJ, Gnecchi M, Pachori AS, Morello F, Melo LG. Therapeutic potential of endothelial progenitor cells in cardiovascular diseases. *Hypertension.* 2005;46:7-18.

10. Pislaru SV, Van Ranst M, Pislaru C, Szelid Z, Theilmeier G, Ossewaarde JM, Holvoet P, Janssens S, Verbeken E, Van de Werf FJ. Chlamydia pneumoniae induces neointima formation in coronary arteries of normal pigs. *Cardiovasc Res.* 2003;57:834-842.

11. Moore XL, Lu J, Sun L, Zhu CJ, Tan P, Wong MC. Endothelial progenitor cells' "homing" specificity to brain tumors. *Gene Ther.* 2004;11:811-818.

12. Zhu X, Rodriguez-Porcel M, Bentley MD, Chade AR, Sica V, Napoli C, Caplice N, Ritman EL, Lerman A, Lerman LO. Antioxidant intervention attenuates myocardial neovascularization in hypercholesterolemia. *Circulation.* 2004;109:2109-2115.

13. Zhu XY, Chade AR, Rodriguez-Porcel M, Bentley MD, Ritman EL, Lerman A, Lerman LO. Cortical Microvascular Remodeling in the Stenotic Kidney. Role of Increased Oxidative Stress. *Arterioscler Thromb Vasc Biol.* 2004;24:1854-1859.

14. Bentley MD, Rodriguez-Porcel M, Lerman A, Sarafov MH, Romero JC, Pelaez LI, Grande JP, Ritman EL, Lerman LO. Enhanced renal cortical vascularization in experimental hypercholesterolemia. *Kidney Int.* 2002;61:1056-1063.

15. Chade AR, Bentley MD, Zhu X, Rodriguez-Porcel M, Niemeyer S, Amores-Arriaga B, Napoli C, Ritman EL, Lerman A, Lerman LO. Antioxidant intervention prevents renal neovascularization in hypercholesterolemic pigs. *J Am Soc Nephrol.* 2004;15:1816-1825.

16. Chade AR, Rodriguez-Porcel M, Grande JP, Zhu X, Sica V, Napoli C, Sawamura T, Textor SC, Lerman A, Lerman LO. Mechanisms of renal structural alterations in combined hypercholesterolemia and renal artery stenosis. *Arterioscler Thromb Vasc Biol.* 2003;23:1295-1301.

17. Krier JD, Ritman EL, Bajzer Z, Romero JC, Lerman A, Lerman LO. Noninvasive measurement of concurrent single-kidney perfusion, glomerular filtration, and tubular function. *Am J Physiol Renal Physiol.* 2001;281:F630-638.

18. Daghini E, Primak AN, Chade AR, Krier JD, Zhu X, McCollough CH, Lerman LO. Assessment of renal hemodynamics and function using 64-slice multidetector CT: comparison with EBCT. *Radiology.* 2007;243:405-412.

19. Chade AR, Rodriguez-Porcel M, Grande JP, Krier JD, Lerman A, Romero JC, Napoli C, Lerman LO. Distinct renal injury in early atherosclerosis and renovascular disease. *Circulation.* 2002;106:1165-1171.

20. Chade AR, Rodriguez-Porcel M, Herrmann J, Krier JD, Zhu X, Lerman A, Lerman LO. Beneficial Effects of Antioxidant Vitamins on the Stenotic Kidney. *Hypertension.* 2003;42:605-612.

21. Chade AR, Rodriguez-Porcel M, Herrmann J, Zhu X, Grande JP, Napoli C, Lerman A, Lerman LO. Antioxidant intervention blunts renal injury in experimental renovascular disease. *J Am Soc Nephrol.* 2004;15:958-966.

22. Chade AR, Krier JD, Rodriguez-Porcel M, Breen JF, McKusick MA, Lerman A, Lerman LO. Comparison of Acute and Chronic Antioxidant Interventions in Experimental Renovascular Disease. *Am J Physiol Renal Physiol.* 2004;286:F1079-1086.

Figure legends

Figure 1s: Antigenic and functional characterization of cultured autologous EPC.

Top right: bar graph showing similar quantity of colony forming units in normal and RAS animals.

Left and bottom right: Expression of monocytic (CD14), progenitor (CD34, CD133), endothelial (KDR), and stem (Oct-4) cell markers. The expression of CD14 and CD133 decreased with cellular maturation, while the expression of KDR increased, suggesting the EPC acquired endothelial phenotype. The expression of Oct-4 was evident in both early and late cells as well, suggesting pluripotency of EPC.

Figure 2s: Top**:** Uptake of acetylated LDL by EPC compared to renal tubular cells (used as controls), showing a significant uptake by EPC.

Bottom-left**:** Migratory function of endothelial progenitor cell (EPC) of normal and RAS pigs.

Bottom-right: The MTS assay shows increased late EPC proliferation in RAS. *p<0.05 vs. Normal

Figure 3s: Angiogenic ability of endothelial progenitor cells of normal and RAS pigs.

Top: DiI-labeled EPC (red) incorporate into tubes formed by HUVEC (grey). Bottom: quantitative tube number (tubes per field) and length. *p<0.05 vs. normal.

Figure 4s: Left: vascular endothelial growth factor (VEGF) levels in culture media of endothelial progenitor cells isolated from normal and RAS pigs. Right: densitometry and representative immunoblots of VEGF and eNOS in endothelial progenitor cells isolated from normal and RAS pigs, showing increased VEGF and eNOS expression in RAS pigs. *p<0.05 vs. normal

Figure 5s: Top and middle: representative perivascular (top) and peritubular (middle) double fluorescence of CM-DiI (red) and immunoreactivity of CD31 (green, x40) in frozen RAS+EPC kidney sections 4 weeks after renal injection. EPC were integrated into small vessels or capillaries (dash arrows), but not in larger vessels (white arrow). Bottom: RAS+EPC kidney sections stained with cytokeratin (green) and CM-DiI labeled EPC (red). Some injected EPC showed expression of CD31 or cytokeratin, suggesting that they assumed endothelial and tubular characteristics.

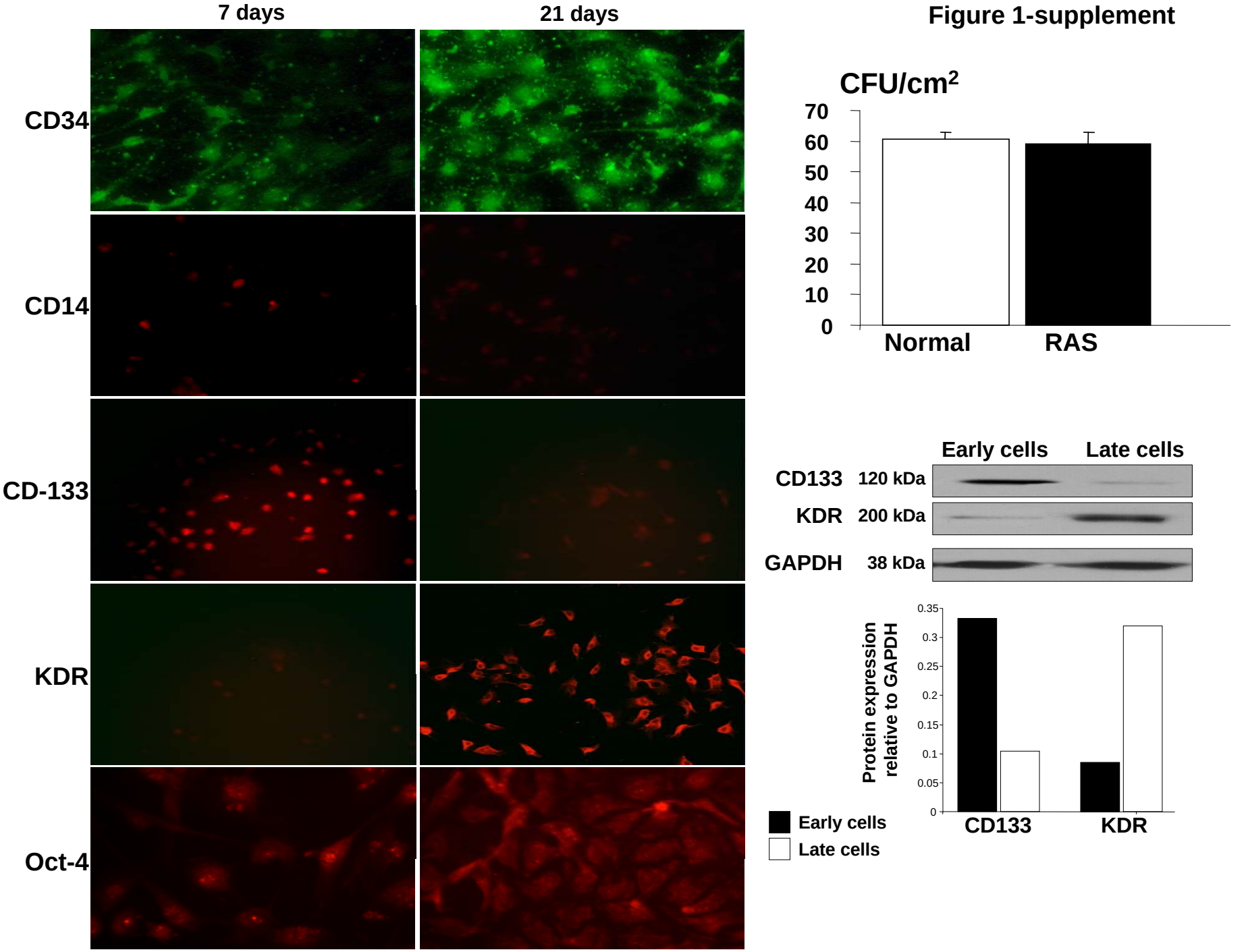
7 days
21 days
CD34
CD14
CD-133
KDR
Oct-4
Figure 1-supplement
CFU/cm2
70
60
50
40
30
20
10
0
Normal
RAS
Early cells
Late cells
CD133
120 kDa
KDR
200 kDa
GAPDH
38 kDa
Protein expression relative to GAPDH
0.35
0.3
0.25
0.2
0.15
0.1
0.05
0
CD133
KDR
Early cells
Late cells

Figure 2-supplement

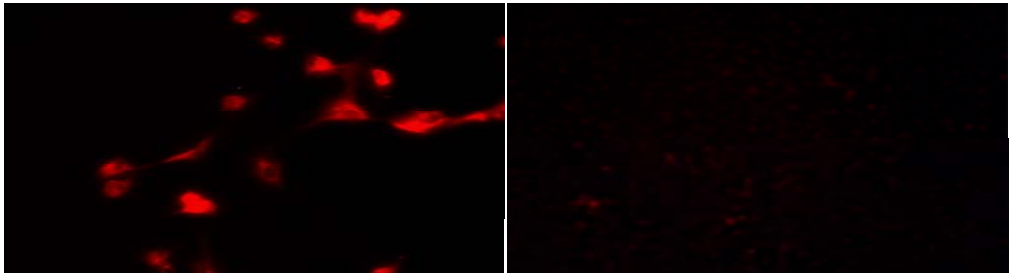

Acetylated LDL uptake

Controls

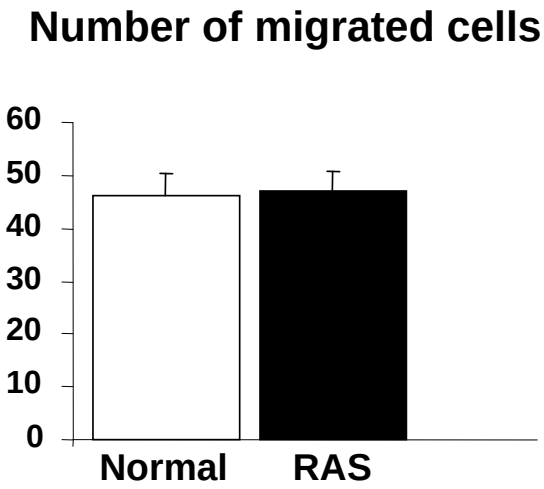

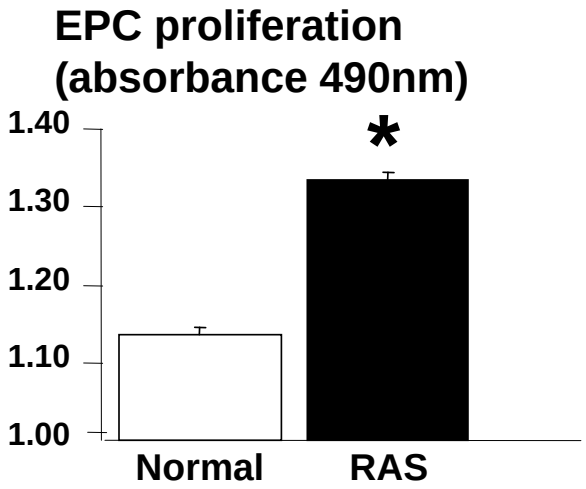

Figure 3-supplement

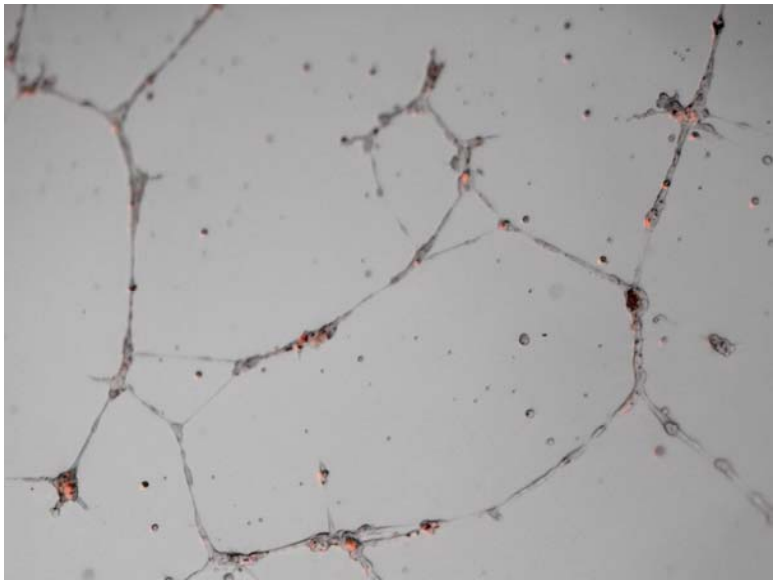

Normal

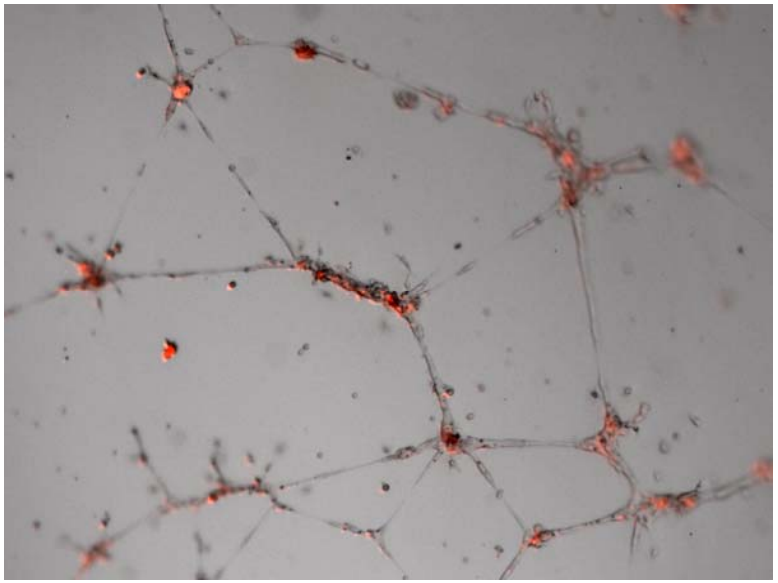

RAS

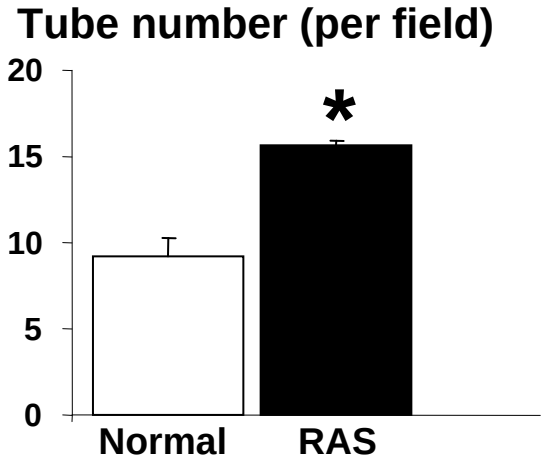

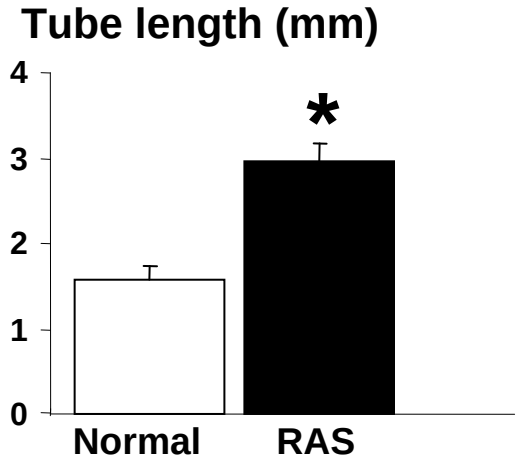

Figure 4-supplement

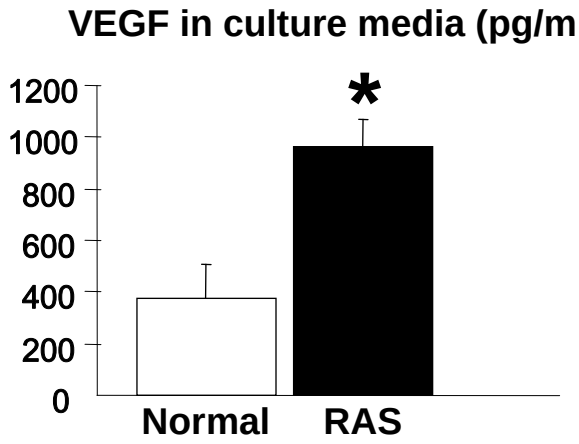

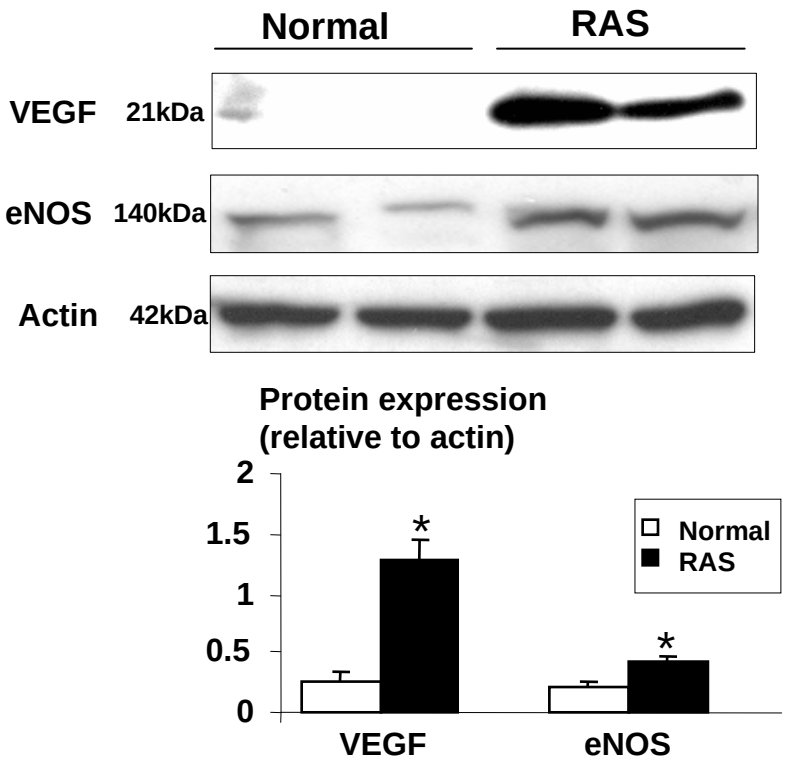

Figure 5-supplement